Spectroscopic Identification of Carbenium and Ammonium Isomers of Protonated Aniline (AnH^+): IR Spectra of Weakly Bound AnH^+-L_n Clusters (L = Ar, N_2)

Felix M. Pasker, Nicola Solcà,† and Otto Dopfer*

Institut für Optik und Atomare Physik, Technische Universität Berlin, Hardenbergstrasse 36, D-10623 Berlin, Germany

Received: July 19, 2006; In Final Form: September 9, 2006

Infrared photodissociation (IRPD) spectra of mass-selected clusters composed of protonated aniline ($C_6H_8N^+$ = AnH^+) and a variable number of neutral ligands (L = Ar, N_2) are obtained in the N−H stretch range. The AnH^+-L_n complexes ($n \leq 3$) are produced by chemical ionization in a supersonic expansion of An, H_2, and L. The IRPD spectra of AnH^+-L_n feature the unambiguous fingerprints of at least two different AnH^+ nucleation centers, namely, the ammonium isomer (**5**) and the carbenium ions (**1** and/or **3**) corresponding to protonation at the N atom and at the C atoms in the para and/or ortho positions, respectively. Protonation at the meta and ipso positions is not observed. Both classes of observed AnH^+-L_n isomers exhibit very different photofragmentation behavior upon vibrational excitation arising from the different interaction strengths of the AnH^+ cores with the surrounding neutral ligands. Analysis of the incremental N−H stretch frequency shifts as a function of cluster size shows that microsolvation of both **5** and **1**/**3** in Ar and N_2 starts with the formation of intermolecular H bonds of the ligands to the acidic NH protons and proceeds by intermolecular π bonding to the aromatic ring. The analysis of both the photofragmentation branching ratios and the N−H stretch frequencies demonstrates that the N−H bonds in **5** are weaker and more acidic than those in **1**/**3**, leading to stronger intermolecular H bonds with L. The interpretation of the spectroscopic data is supported by density functional calculations conducted at the B3LYP level using the 6-31G* and 6-311G(2df,2pd) basis sets. Comparison with clusters of neutral aniline and the aniline radical cation demonstrates the drastic effect of protonation and ionization on the acidity of the N−H bonds and the topology of the intermolecular potential, in particular on the preferred aromatic substrate−nonpolar ligand recognition motif.

Introduction

Protonation of aromatic molecules is of central importance to many chemical and biological phenomena. For instance, protonated aromatic molecules (AH^+) are invoked as short-lived intermediates in ionic chemical reaction mechanisms, such as the electrophilic aromatic substitution reaction.[1−7] Fundamental properties of the protonation process of aromatic molecules (energetics, dynamics, favorable protonation site) depend sensitively on several factors, such as physical conditions (pressure, temperature), the method for AH^+ preparation, solvation effects, and the substitution of functional groups. Studies of AH^+ ions isolated in the gas phase are required to separate their intrinsic properties from the substantial solvation effects. In addition, investigations of size-selected AH^+-L_n clusters, in which a variable number (n) of neutral ligands (L) are attached to a central AH^+ ion, are ideal targets to establish the effects of stepwise microsolvation on the properties of AH^+ and to bridge the gap toward the condensed phase. To this end, a plethora of gas-phase studies have been carried out to characterize the properties of AH^+ ions.[6,8−11] However, these studies are mainly based on mass spectrometry and the radiolytic approach and thus provide only indirect and sometimes ambiguous information about the potential energy surface, in particular about the preferred protonation site in AH^+ ions. Recent advances in the development of sensitive infrared (IR) spectroscopic techniques, coupled to selective mass spectrometric methods, have allowed for the first time for the unambiguous structural characterization of the protonation process of isolated and microsolvated AH^+ ions[12,13] by direct comparison of experimental IR spectra with those calculated with quantum chemical techniques. All successful approaches rely on infrared photodissociation (IRPD) schemes performed in tandem mass spectrometers, and details of their application to (microsolvated) AH^+ ions are described in a recent review.[14] The two major experimental strategies involve (i) single-photon IRPD spectroscopy of AH^+ or AH^+-L_n ions in a tandem quadrupole mass spectrometer using novel optical parametric oscillator laser systems in the 2500−4000 cm^{-1} range[12,13,15−24] and (ii) IR multiphoton dissociation (IRMPD) spectroscopy in a Fourier transform ion cyclotron resonance mass spectrometer or a quadrupole ion trap using high-intensity free electron lasers in the 500−2500 cm^{-1} range.[25−32]

In the present work we report IRPD spectra of size-selected AnH^+-L_n complexes, in which protonated aniline (AnH^+) is solvated by a controlled number ($n \leq 3$) of neutral ligands (L = Ar, N_2). The spectra obtained correspond to the first spectroscopic data for clusters with protonated aniline as a chromophore. Thus, they provide a first impression of the potential energy surface of protonated arylamines interacting with neutral molecules. Aniline is the most simple molecule to investigate the competition between protonation of an amino group and an aromatic ring. Consequently, AnH^+-L_n clusters

* To whom correspondence should be addressed. Fax: (+49) 30-314-23018. Phone: (+49) 30-314-23017. E-mail: dopfer@physik.tu-berlin.de.
† Present address: Laboratorio Cantonale, Via Mirasole 22, CH-6500 Bellinzona, Switzerland.

10.1021/jp064571a CCC: $33.50
Published on Web 11/09/2006

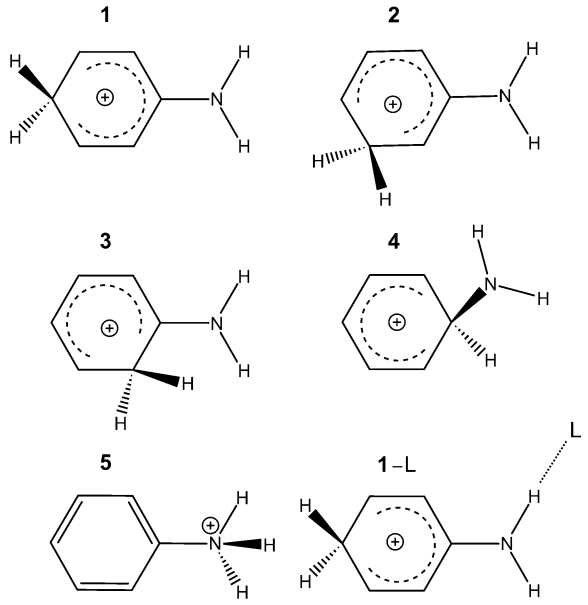

Figure 1. Structures of AnH^+ isomers and H-bound AnH^+-L dimers. Protonation of aniline may occur at the aromatic ring in the para (**1**, C_{2v}), meta (**2**, C_s), ortho (**3**, C_s), and ipso (**4**, C_s) positions to form carbenium ions or at the nitrogen atom (**5**, C_s) to form the ammonium ion. The energetic difference between the two rotamers of **5** having one N−H bond either in the aromatic plane (**5b**, shown in the figure) or rotated by 90° (**5a**, not shown) is negligible. H bonding of ligands L to the acidic NH protons corresponds to the dominant ion−ligand binding motif. As an example, the H-bonded complex of **1**−L (C_s) is shown.

with L = Ar and N_2 are model systems to characterize the interaction of protonated arylamines with a nonpolar, hydrophobic, aprotic environment. Although aniline is well-known to protonate at the N atom in aqueous and superacid solutions,[1−3,33−35] the preferred protonation site in the gas phase is still unclear. Hence, microsolvated clusters of AnH^+ are ideal model systems to investigate the strong impact of solvation on the protonation behavior. There are two major competing binding sites for the interaction between AnH^+ and the surrounding solvent molecules. The ligands L can either form a hydrogen bond to one of the acidic protons (H bond) or bind to the aromatic π electron system of the aromatic ring (π bond). Other binding sites are significantly less stable.[36,37] The IRPD spectra of AnH^+-L_n are recorded in the N−H stretch range and thus provide detailed information about the strength and acidity of the N−H bonds, the strength of the ion−ligand interaction, and the preferred intermolecular ion−ligand binding motif as a function of the solvent type, the degree of solvation, and the protonation site. Comparison with the corresponding spectra of clusters of neutral aniline[38−41] and the aniline radical cation[40,42,43] demonstrates the significant effects of both ionization and protonation on the intermolecular aromatic molecule−hydrophobic ligand recognition motif and the acidity of the NH proton donors.[44]

Possible AnH^+ structures are illustrated in Figure 1. Protonation of aniline can occur at the C atoms of the aromatic ring in the para, meta, ortho, and ipso positions to form the carbenium ions **1**−**4** (aminobenzenium) and at the N atom to form the ammonium ion **5** (phenylammonium, anilinium). Only σ complexes (C or N protonation of aniline, **1**−**5**) are considered, because π complexes of aromatic molecules with small electrophiles (such as H^+) are saddle points on the AH^+ potential.[15,45] This is in contrast to a variety of metal cation complexes of aniline ($An-Me^+$, with Me = alkali or transition metals)

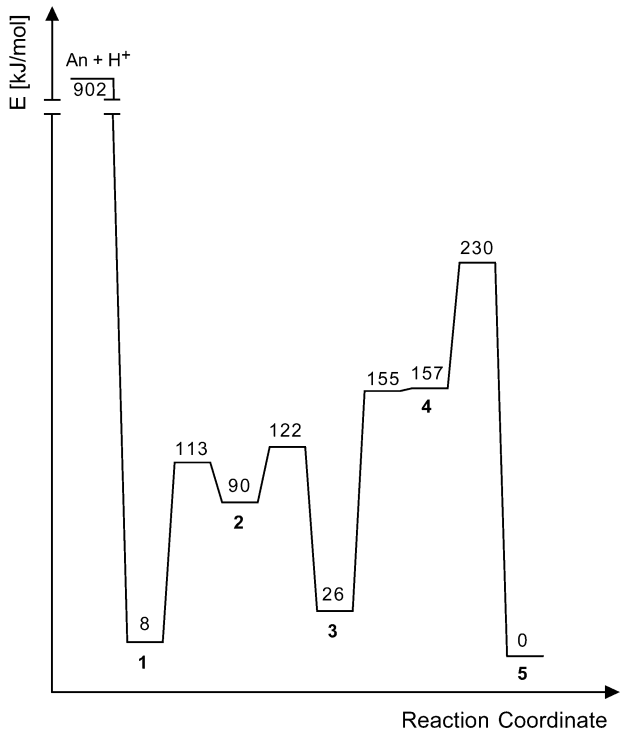

Figure 2. Salient parts of the potential energy surface of AnH^+ calculated at the B3LYP/6-311G(2df,2pd) level. Relative energies (E_{rel}, kJ/mol) given with respect to **5** are corrected for zero-point energy.

for which π complexes are minima on the potential energy surfaces and energetically competitive with σ complexes involving N−Me bonds.[46−49] Previous quantum chemical calculations reveal that the preferred protonation site strongly depends on the theoretical level employed.[34,50−57] All sophisticated calculations, however, agree that **1** and **5** are similar in energy (to within a few kilojoules per mole at the highest level of calculations), whereas **2**−**4** are significantly less stable. Figure 2 shows the potential energy surface of AnH^+ obtained at the B3LYP/6-311G(2df,2pd) level in the present work. At this level, the relative energies vary in the order **5** < **1** < **3** ≪ **2** ≪ **4**; that is, both N and ring protonations in the ortho or para position are relatively close in energy. It has been noted that the energy ordering of the AnH^+ isomers may also easily be affected by solvation.[34,51,54,58,59] In particular, the ammonium isomer **5** may be preferentially lowered in energy with respect to the carbenium isomers **1**−**4**, because the highly localized charge in **5** can be better stabilized by solvation than the extensively delocalized charge in **1**−**4**. Similarly, the substitution of functional groups can heavily affect the relative energies of carbenium and ammonium isomers.[51,52,57,58,60−62]

The numerous experimental studies available for isolated AnH^+ are all based on mass spectrometric techniques.[50,54−56,58,60−69] The results were interpreted with the presence of ring- and/or N-protonated AnH^+ isomers, although the exact protonation site on the ring could not be determined. In addition, the preference for C or N protonation strongly varies with the experimental conditions, in particular with the method of generation (e.g., precursor, protonating agent, pressure, temperature, degree of complexation). Despite the plethora of available mass spectrometrical data, their analysis is still inconclusive about the energetically most favorable protonation site (C or N) and in particular about the preferred C atom in the carbenium isomers. The analysis of the evaporation kinetics and magic numbers in mass spectra of large $AnH^+-(H_2O)_n$ clusters generated in an electrospray ionization source indicated that N protonation of AnH^+

in nanodroplets is favored in a microhydration environment.[54] Similarly, NMR spectra of AnH^+ in superacid solutions suggest that anilines are N protonated in the liquid phase,[33] in agreement with calculations which predict isomer **5** of AnH^+ to be about 50 kJ/mol more stable than **1** in aqueous solution.[34] The present work on AnH^+-L_n clusters presents the first spectroscopic attempt to unambiguously determine the protonation sites observed for isolated and microsolvated AnH^+.

Experimental and Computational Methods

IRPD spectra of mass-selected AnH^+-L_n complexes (L = Ar, N_2; $n \leq 3$) are recorded in a tandem quadrupole mass spectrometer (QMS1/2) coupled to a cluster ion source and an octopole ion trap.[70] Briefly, the cluster ions are produced in a pulsed supersonic plasma expansion obtained by electron and chemical ionization in a molecular beam. The gas mixture, generated by passing carrier gas of the composition H_2/L in a ratio of 1:20 at room temperature and stagnation pressures of $p_s = 5-15$ bar through a reservoir filled with aniline, expands through a pulsed nozzle into a vacuum chamber. Electron ionization of the gas mixture close to the nozzle orifice is achieved by two electron beams ($E \approx 100$ eV) emitted from heated tungsten filaments. Ion−molecule reactions in the high-pressure region of the expansion form Brønsted acids XH^+ (e.g., X = H_2 and L), which subsequently protonate aniline via rapid exothermic proton transfer:[12,13]

$$XH^+ + An \rightarrow X + AnH^+ \qquad (1)$$

An alternative route for the production of AnH^+ involves electron ionization of neutral An_n clusters prepared in the molecular beam followed by intracluster proton transfer and evaporative cooling.[13] However, the lack of AnH^+ ions in mass spectra for similar expansions without H_2 in the carrier gas[42,43] demonstrates that this mechanism plays only a minor role under the employed ion source conditions. Similarly, bimolecular self-protonation reactions[71] can be neglected. After AnH^+ generation, weakly bound AnH^+-L_n aggregates are formed by three-body association reactions in the collision-rich region of the expansion:

$$AnH^+-L_{n-1} + L + M \rightarrow AnH^+-L_n + M \ (M = L, An, H_2) \qquad (2)$$

As an example, Figure 3 shows a mass spectrum of the ion source for an expansion of aniline vapor in H_2/N_2 at $p_s = 5$ bar. The mass spectrum is dominated by N_n^+ ions (with the expected even−odd intensity alternation, open circles)[19,36,43,72−74] and $(N_2)_nH^+$ clusters (filled circles), as well as An^+ (open triangles) and AnH^+ (filled triangles) and their weakly bound N_2 clusters (vertically expanded inset in Figure 3). The intensity ratio of the AnH^+ ($m = 94$ u) and An^+ ($m = 93$ u) mass peaks of ∼2.5 confirms the efficient protonation of An via reaction 1, mainly achieved with XH^+═H_3^+ and $(N_2)_nH^+$. The intensity ratio of AnH^+ ($m = 94$ u) and AnH^+-N_2 ($m = 122$ u) of ∼60 is indicative of the generation of weakly bound $AnH^+-(N_2)_n$ ion−ligand complexes.

The central part of the plasma expansion is extracted from the ion source through a skimmer into QMS1, which is tuned to the mass of the AnH^+-L_n cluster under investigation. The mass-selected AnH^+-L_n parent ion beam is subsequently injected into an octopole ion guide where it interacts with a tunable IR laser pulse generated by an optical parametric oscillator laser system. Resonant vibrational excitation of

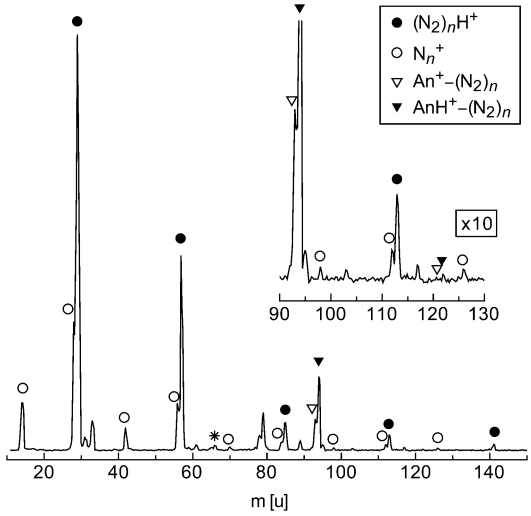

Figure 3. Mass spectrum of the electron ionization source obtained for an expansion of H_2/N_2 (ratio 1:20) and aniline vapor at $p_s = 5$ bar. The intense signals of N_n^+ and $(N_2)_nH^+$ are indicated by open and filled circles, respectively. An^+ and AnH^+, as well as their N_2 clusters, are marked by open and filled triangles, respectively. Part of the spectrum is vertically expanded by a factor of 10 to visualize smaller peaks, such as those for the AnH^+-N_2 clusters. The asterisk indicates the strongest fragment of An upon electron ionization ($m = 66$ u, HNC loss).[123]

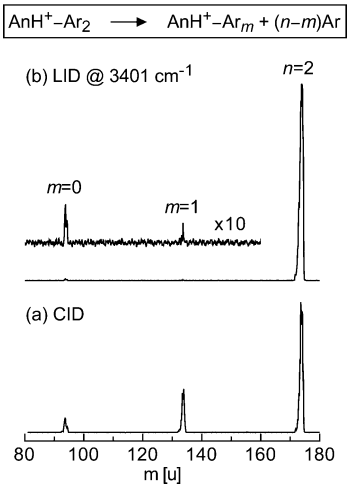

Figure 4. Mass spectra obtained by selecting AnH^+-Ar_2 clusters with QMS1 and scanning QMS2 to detect AnH^+-Ar_m ($m < 2$) fragments. Spectrum a is obtained by introducing 10^{-5} mbar of N_2 gas into the octopole, which induces CID into the $m = 0$ and $m = 1$ fragment channels. Spectrum b is recorded with resonant LID (at $\nu_{IR} = 3401$ cm^{-1}). Part of the spectrum is vertically expanded by a factor of 10 to visualize the small fragment peaks arising from metastable decay ($m = 1$) and LID ($m = 0$).

AnH^+-L_n induces the rupture of one or more intermolecular bonds according to

$$AnH^+-L_n + h\nu_{IR} \rightarrow AnH^+-L_m + (n-m)L \qquad (3)$$

No other fragment channel is observed under the single-photon absorption conditions employed.[12,75] The AnH^+-L_m fragment ions are selected by QMS2 and monitored as a function of the laser frequency (ν_{IR}) to obtain the IRPD spectrum of the AnH^+-L_n parent cluster. As an example, Figure 4 shows mass spectra obtained by mass selecting AnH^+-Ar_2 with QMS1 and scanning QMS2 to detect AnH^+-Ar_m fragment ions with $m < 2$. Spectrum a is obtained by introducing $\sim 10^{-5}$ mbar of N_2 gas into the octopole region, which induces collision-induced

dissociation (CID; ~1 eV center-of-mass collision energy) into the $m = 0$ and $m = 1$ fragment channels. The exclusive observation of the loss of one and two Ar atoms upon CID indicates that the ions with $m = 174$ u selected with QMS1 are indeed only clusters of the type AnH^+-Ar_2. Spectrum b is recorded without collision gas in the octopole ($p < 10^{-7}$ mbar) but with resonant laser-induced dissociation (LID; at $\nu_{IR} = 3401$ cm^{-1}, resonance B_1). Part of the spectrum is vertically expanded by a factor of 10 to visualize the small fragment peaks arising from metastable decay and LID in the octopole region. The $m = 1$ fragment peak arises solely from metastable decomposition, and its low intensity (~0.3% of $n = 2$) suggests that the AnH^+-Ar_2 parent ions probed in the octopole are rather cold. The $m = 0$ fragment peak (~1% of $n = 2$) is merely produced by resonant LID, and its weak intensity is indicative of the relatively low efficiency for this process under the present experimental conditions. For larger AnH^+-L_n clusters ($n > 1$) several LID channels, $m < n$, may be observed, and this information has proven to be useful for both isomer identification[19,21,76] and evaluation of experimental ligand binding energies.[44] For AnH^+-L_n (L = Ar, N_2) with $n \leq 2$, all LID signals occur in the AnH^+ channel ($m = 0$). However, LID of $AnH^+-(N_2)_3$ clusters is observed in both the $m = 0$ and $m = 1$ channels, which turns out to be key information for assigning the features observed in the IRPD spectra of all clusters investigated. Consequently, the $m = 0$ and 1 fragment channels of $AnH^+-(N_2)_3$ are monitored in the same scan by switching the mass of QMS2 for each IR laser frequency. Calibration of ν_{IR} is accomplished by recording optoacoustic spectra of ammonia[77] simultaneously with the IRPD spectra.

To facilitate the assignments of the vibrational bands observed in the IRPD spectra, density functional theory calculations of AnH^+-L_n are carried out at the B3LYP/6-31G* level of theory.[78] This level qualitatively reproduced the intermolecular interaction and complexation-induced frequency shifts for related H-bonded $A(H)^+-L_n$ complexes with L = Ar and N_2, such as A = phenol,[13,79] aniline,[42,43] and indole.[73] The properties of the isolated AnH^+ isomers are also investigated at the B3LYP/6-311G(2df,2pd) level. This level provides a reliable description of the potential energy surface of isoelectronic protonated phenol, with an accuracy similar to that of the MP2/6-311G(2df,2pd) level.[18] In general, all coordinates are relaxed during the search of stationary points. The identification of minima and transition states is verified by harmonic frequency analysis. Intermolecular interaction energies are counterpoise corrected for basis set superposition error.[80] Harmonic frequencies are employed to correct energies for vibrational zero-point motion. The population analysis of the charge distribution in the various AnH^+ isomers is carried out using the atoms-in-molecules (AIM) approach (6-31G* basis set).

Quantum Chemical Results

Figure 2 summarizes the salient parts of the potential energy surface of protonated aniline evaluated at the B3LYP/6-311G(2df,2pd) level. Only σ complexes corresponding to C and N protonation are considered, because π complexes of protonated aromatic molecules are saddle points on the potential.[15,45,81] Similar to that of isoelectronic toluene,[82,83] the barrier for internal rotation of the NH_3 group in the anilinium ion is rather low. The energetic difference between the two rotamers having one N−H bond in the aromatic plane (**5b**, shown in Figure 1) or rotated by 90° (**5a**) is calculated to be only 0.3 kJ/mol. The relative energies of the carbenium and ammonium isomers vary in the order **5** < **1** < **3** ≪ **2** ≪ **4** (0 < 8 < 26 ≪ 90 ≪ 157 kJ/mol); that is, both N and ring protonations in the ortho and para positions are close in energy. The latter observation is consistent with the ortho/para-directing nature of the amino group in electrophilic aromatic substitution.[1,2] Interestingly, the energy order of **1** and **5** is reversed at the B3LYP/ 6-31G* level (**1** < **5** < **3** ≪ **2** ≪ **4**, 0 < 13 < 17 < 97 < 169 kJ/mol), indicating that the relative energies for ring and substituent protonation are sensitive to the theoretical level employed. A similar basis set effect was recently also noted for the relative energies of ring and O protonation of phenol, for which also the larger basis set resulted in a significant additional stabilization of the oxonium ion with respect to the carbenium isomers.[18] The interconversion between **1**, **3**, and **5** of AnH^+ involves very high isomerization barriers (96−230 kJ/mol), suggesting that these three isomers could readily be produced and collisionally stabilized in observable concentrations in the employed plasma expansion. In contrast, protonations in the meta and ipso positions are energetically unfavorable processes and require less than 35 kJ/mol for isomerization toward either **1** or **3**. Hence, the concentration of **2** and **4** in the molecular beam is expected to be small. In fact, although vibrational frequency analysis of **1**−**5** confirms their identification as minima on the potential, **4** appears to become unstable with respect to intramolecular 1,2 H-shift toward **3** after inclusion of zero-point energy corrections. Hence, ipso protonation is not considered further for the evaluation of the spectroscopic properties of the AnH^+-L_n clusters. The calculated proton affinity of 901.6 kJ/mol for N protonation compares reasonably well with previous higher level calculations (878,[54] 876,[51] 885,[57] 877,[55] 876,[56] and 874[53] kJ/mol) as well as the experimental value (882.5 kJ/mol),[84] although the exact protonation site is not well-known in the experimental studies.

Table 1 summarizes the properties of the N−H bonds in the AnH^+ isomers **1**−**5**, such as bond lengths (R_{NH}), harmonic stretch frequencies (ω_{NH}), and IR intensities (I_{NH}). As will be shown, the differences in these properties are significant for certain AnH^+ isomers and will be used below to identify different isomers in the experimental IRPD spectra of the AnH^+-L_n clusters. The N−H bond lengths are similar for **1** and **3** (~1.0093 Å), significantly shorter for **2** (~1.0043 Å), substantially longer for **4** (~1.0104 Å), and longest for both rotamers of **5** (~1.0232 Å). These N−H bond length variations translate directly into differences in the frequencies of the corresponding N−H stretch normal modes. The carbenium ions feature two (nearly) degenerate local N−H stretch modes, which via vibrational coupling result in a lower frequency symmetric and a higher frequency antisymmetric N−H stretch normal mode, ω_{NH}(s) and ω_{NH}(as). The splitting between both normal modes is on the order of 100 cm^{-1} for all carbenium isomers, and the absolute frequencies follow the order **2** > **1** ≈ **3** > **4**. The three N−H stretch normal modes of both rotamers of **5** are quite similar (with differences of less than 2 cm^{-1} for **5a** and **5b**), indicating that the nearly free internal rotation of the NH_3 group has almost no effect on the geometric and vibrational coupling parameters of the N−H bonds. In general, the N−H stretch frequencies of **5** are, however, significantly lower than those of all carbenium isomers, due to the much longer and weaker N−H bonds in the former ions. Significantly, the calculated IR stick spectra of isomers **1**−**5** in the N−H stretch range (Figure 5) clearly demonstrate that, with the exception of **1** and **3**, all AnH^+ isomers can unambiguously be distinguished by their N−H stretch spectra. This is in contrast to the relative energies, which are quite similar for the three most stable and thus most relevant isomers **1**, **3**, and **5** (Table 1, Figure 2).

TABLE 1: Selected Properties of AnH^+ Isomers Evaluated at the B3LYP/6-311G(2df,2pd) Level: Relative Energies (E_{rel}), N−H and Aliphatic C−H Bond Separations (R_{NH}, R_{CH}), and N−H Stretch, Aliphatic C−H Stretch, and Selected N−H Bend Frequencies (ω_{NH}, ω_{CH}, ω_b)[a]

AnH^+	E_{rel}[b] (kJ/mol)	R_{NH} (Å)	ω_{NH}[c] (cm^{-1})	$R_{CH}(sp^3)$ (Å)	$\omega_{CH}(sp^3)$[c] (cm^{-1})	ω_b[c] (cm^{-1})
1 (C_{2v})	8.1	1.0093	3663 (b_2, 88)	1.1001	2993 (b_1, 5)	1702 (a_1, 428)
		1.0093	3553 (a_1, 228)	1.1001	2989 (a_1, 19)	
2 (C_s)	89.9	1.0044	3720 (a′, 60)	1.1064	2944 (a′, 51)	1673 (a′, 223)
		1.0041	3607 (a′, 159)	1.1064	2935 (a″, 21)	
3 (C_s)	26.4	1.0090	3661 (a′, 84)	1.0978	3024 (a″, 5)	1700 (a′, 263)
		1.0096	3551 (a′, 222)	1.0978	3005 (a′, 12)	
4 (C_s)	156.6	1.0104	3627 (a″, 32)	1.1681	2423 (a′, 64)	1671 (a′, 65)
		1.0104	3539 (a′, 66)			
5a (C_s)	0	1.0226	3473 (a″, 84)			1653 (a′, 46)
		1.0226	3451 (a′, 102)			
		1.0243	3385 (a′, 56)			
5b (C_s)	0.3	1.0222	3474 (a′, 83)			1652 (a″, 43)
		1.0237	3449 (a″, 106)			
		1.0237	3386 (a′, 55)			
An (C_s)	902	1.0073	3657 (a″, 11)			1664 (a″, 127)
		1.0073	3562 (a′, 13)			
An^+ (C_{2v})		1.0108	3647 (b_2, 92)			1676 (a′, 109)
		1.0108	3535 (a_1, 251)			

[a] Corresponding data for An and An^+ are also included. [b] Corrected for zero-point energy. [c] IR intensities I_{NH}, I_{CH}, and I_b (km/mol) as well as vibrational symmetry species are listed in parentheses.

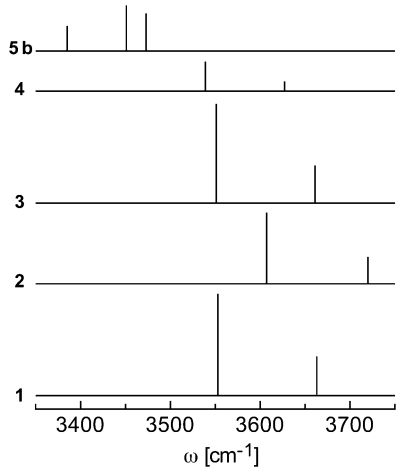

Figure 5. Theoretical IR stick spectra of the N−H stretch vibrations of all possible AnH^+ isomers calculated at the B3LYP/6-311G(2df,2pd) level (Table 1).

In addition to the N−H bond lengths and stretch frequencies, the positive partial charges on the amino protons, q_H, provide a measure for the acidity of the NH protons and their ability to form H bonds to neutral ligands.[16] The AIM charges increase in the order **2** < **1** ≈ **3** < **5** (q_H/e = 0.45 < 0.47 ≈ 0.47 < 0.49). Hence, the weaker and longer the N−H bonds, the lower the ω_{NH} values, the larger the q_H values, and the more acidic the NH protons in the various AnH^+ isomers.

Table 1 also compares the bond lengths (R_{CH}) and the two C−H stretch frequencies of the aliphatic CH_2 groups of the carbenium isomers (ω_{CH}). The CH_2 group corresponds to the reactive center of these arenium ions in the electrophilic aromatic substitution reaction mechanism. The bond lengths, R_{CH}, vary in the order **4** > **2** > **1** ≈ **3**, and the corresponding frequencies, ω_{CH}, show the opposite trend, **4** < **2** < **1** ≈ **3**. Interestingly, these trends are also roughly reflected in the relative energies of the carbenium isomers, E_{rel}, which decrease in the order **4** > **2** > **3** ≈ **1**. Apparently, the bond lengths and vibrational frequencies of the aliphatic CH_2 group provide a rough indicator for the acidity and corresponding proton affinity of the arenium ions for the various protonation sites.[22] The fact that this correlation does not strictly hold for the energetically close lying isomers **1** and **3** is probably due to slight differences between the CH_2 normal coordinates and the effective reaction coordinate for the ring protonation process. In general, the IR intensities of the aliphatic C−H stretch vibrations are significantly lower than those of the intense N−H stretch modes. The aromatic C−H stretch modes occur to slightly higher frequency than the aliphatic ones and feature even lower IR intensities. Consequently, both types of C−H stretch modes are not observed in the experimental IRPD spectra of AnH^+-L_n discussed below and will not be considered further.

In addition to the N−H stretch modes, the IRPD spectra of AnH^+-L_n clusters display the signature of an overtone of a N−H bend vibration, ω_b. For the carbenium isomers **1**−**4**, ω_b corresponds to the in-plane scissoring mode of the NH_2 group. Similarly, for the ammonium ions, ω_b corresponds to a scissoring-type N−H bend mode of the NH_3 group, where two N−H bonds vibrate against the third one. Consequently, their frequencies and IR intensities are also included in Table 1.

The two major ion−ligand binding motifs in small AnH^+-L_n clusters with L = Ar and N_2 involve H bonding of the inert neutral ligands to the acidic NH protons and π bonding to the aromatic ring. Previous combined IRPD spectroscopic and quantum chemical studies of related aromatic $A(H)^+-L_n$ complexes with L = Ar and N_2,[44] including A = (halogenated) phenol,[13,18,19,37,72,79,85] naphthol,[74] aniline,[42,43,86] indole,[73] and imidazole,[36] revealed that H bonding to the acidic functional group is usually preferred over π bonding to the ring. The electrostatic and inductive forces, which favor H bonds, override in these types of clusters the dispersion forces, which favor π bonds.[44] Moreover, H bonds to aliphatic and aromatic CH protons in aromatic $A(H)^+-L_n$ clusters are usually less stable than those to OH and NH protons.[16,44] Hence, the most favorable sequential cluster growth in AnH^+-L_n clusters is expected to begin with the formation of NH−L H bonds to all available NH donors, which is followed by the formation of intermolecular π bonds. The analysis of the experimental AnH^+-L_n spectra is fully consistent with this scenario. Consequently, only H-bonded AnH^+-L_n clusters are investigated computationally in the present work at the B3LYP/6-31G* level of theory. This theoretical level was shown to qualitatively describe the properties of the H bonds in related cluster systems, in particular the complexation-induced vibrational frequency shifts.[43,79]

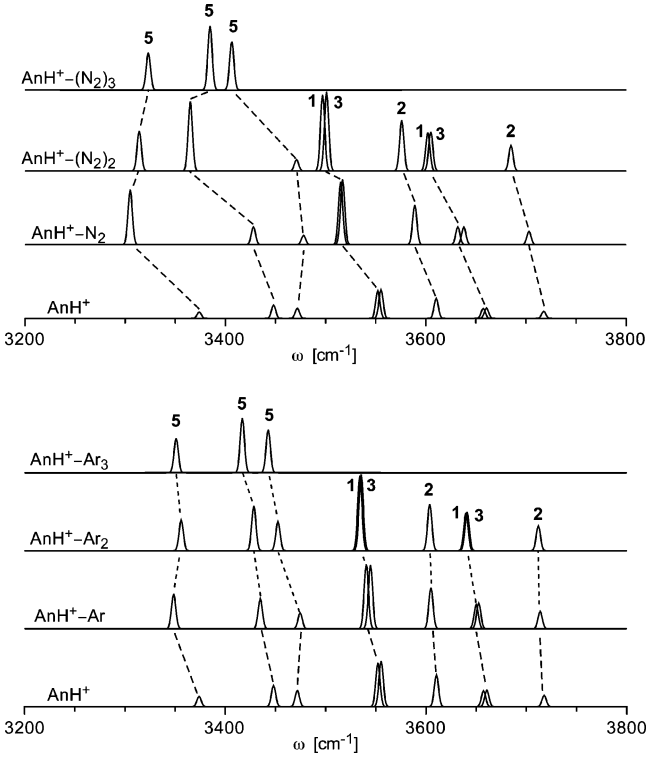

Figure 6. Theoretical IR spectra of the N−H stretch vibrations of AnH^+-L_n ($n \leq 3$) for L = N_2 (top) and L = Ar (bottom) calculated at the B3LYP/6-31G* level using a convolution width of 5 cm^{-1}. Peaks arising from the various AnH^+ isomers **1**−**3** and **5** are indicated. Corresponding transitions are connected by dashed lines. All isomers are assumed to occur with the same abundance.

Intermolecular π bonds in AnH^+-L_n cannot properly be described by B3LYP calculations due to the importance of dispersion forces. Hence, their properties are not evaluated in the present work. On the other hand, previous studies on related systems suggest that the weak intermolecular π bonds have only negligible effects on the vibrational frequencies of the AnH^+ isomers in the considered spectral range (mainly the N−H stretch modes).[16,72]

Sequential H bonding of the available NH protons in both the carbenium and ammonium isomers with Ar and N_2 ligands induces changes of the N−H bond properties which are quite typical for H bonding. Significantly, the proton donor bonds involved in the NH−L H bonds are destabilized and elongated, which leads to a reduction in the frequencies of the corresponding N−H stretch local modes and an IR enhancement. As the N−H stretch modes are strongly coupled in all AnH^+ isomers, all N−H stretch normal modes are somewhat affected upon each H-bonding step. Figure 6 reproduces theoretical IR spectra of the N−H stretch vibrations of AnH^+-L_n ($n \leq 3$) for L = N_2 (top) and L = Ar (bottom) calculated at the B3LYP/6-31G* level. Several isomers are possible for most of the AnH^+-L_n clusters for given L and *n*, arising from the various AnH^+ core ions and the different sequences for solvation of the slightly nonequivalent NH donors. However, as the predicted IR spectra are similar for AnH^+-L_n clusters with the same AnH^+ core but different solvation sequence at the $NH_{2/3}$ group, only one type of isomer is considered for each L and *n*. For **5**−L_n, isomer **5b** is assumed to be the core ion and the solvation sequence begins with H bonding of the first ligand to the N−H bond lying in the aromatic plane of **5b**. For **2**−L_n and **3**−L_n, the solvation is assumed to begin at the N−H bond, which is located in trans orientation to the protonation site. Previous rotationally resolved IRPD spectra of NH_4^+−Rg dimers (Rg = He, Ne, Ar) and NH_3^+−Ar revealed tunneling splittings arising from internal NH_3^+/NH_4^+ rotation.[87−95] As such tunneling motions are largely quenched in **5**−L and **1**/**3**−L due to substitution of a H atom by the aromatic phenyl ring, no splittings are detected in the corresponding IRPD spectra, and thus, no efforts have been undertaken to investigate intermolecular isomerization barriers and resulting tunneling splittings in AnH^+-L. Inspection of Figure 6 reveals that the complexation-induced frequency shifts are larger for $AnH^+-(N_2)_n$ than for AnH^+-Ar_n due to the stronger intermolecular interaction in the former complexes. In addition, as the acidity of the N−H bonds decreases in the order **5** > **1** ≈ **3** > **2**, the H bond strength decreases in the same order. The calculated H bond energies are $D_0/cm^{-1} = 1370 > 895 \approx 907 > 602$ and $410 > 240 \approx 246 > 144$ for the **5**−L, **1**−L, **3**−L, and **2**−L dimers with L = N_2 and Ar, respectively. These binding energies are directly reflected in the intermolecular separations, which increase in the order $R_{HL}/Å = 2.11 < 2.24 \approx 2.23 < 2.33$ and $2.55 < 2.65 \approx 2.64 < 2.73$ for **5**−L, **1**−L, **3**−L, and **2**−L with L = N_2 and Ar, respectively. The dominant contribution to the attractive part of H-bound AnH^+-Ar complexes arises from charge-induced dipole interaction, leading to nearly linear N−H−Ar bonds.[96] The interaction in H-bound AnH^+-N_2 complexes is stronger than in AnH^+-Ar, because of the larger polarizability of N_2 as compared to Ar ($\alpha_{||} = 2.38$ vs 1.64 $Å^3$) and the nonvanishing quadrupole moment of N_2 ($\Theta = -5.00$ C m^2), giving rise to additional charge−quadrupole interaction.[44,97,98] The anisotropy of the long-range charge−quadrupole and charge−induced dipole attraction favors a nearly linear N−H−N−N arrangement in AnH^+-N_2 over a perpendicular approach of the N_2 ligand.[18,36,43,44,71,73,74,79,97−101]

Spectroscopic Results

IRPD Spectra. Figure 7 compares the experimental IRPD spectra of AnH^+-L_n for L = Ar ($n = 1, 2$) and L = N_2 ($n = 1-3$) recorded in the range of the N−H stretch fundamentals (3100−3600 cm^{-1}). The IRPD signals of all clusters investigated occur solely in the AnH^+ channel, with the notable exception of $AnH^+-(N_2)_3$, for which dissociation into both the AnH^+ and AnH^+-N_2 channels is observed (indicated as 3 → 0 and 3 → 1 in Figure 7). The transitions observed are labeled as A_i-D_i, and their positions and suggested vibrational and isomer assignments are listed in Table 2. The 3 → 0 spectrum of $AnH^+-(N_2)_3$ ($m = 178$ u) is slightly contaminated by contributions of $An^+-(N_2)_3$ ($m = 177$ u), because the low signal levels of $AnH^+-(N_2)_3$ required a slight reduction of the mass resolutions of QMS1/2 to increase the ion transmission. The transitions assigned to $An^+-(N_2)_3$ are indicated by asterisks in Figure 7 and could readily be identified by comparison with previous spectroscopic studies of $An^+-(N_2)_n$.[43] In contrast to previous experiments on (protonated) phenol clusters,[18,19] the signal-to-noise levels for the protonated aniline clusters are insufficient to detect the ^{13}C contamination of An^+-L_n clusters[42,43] in the mass channels of the normal isotopomers of the AnH^+-L_n clusters. The typical width of individual vibrational transitions is on the order of 5 cm^{-1}, which mainly arises from unresolved rotational fine structure.

Vibrational and Isomer Assignments. The comparison between the 3 → 0 and 3 → 1 spectra of $AnH^+-(N_2)_3$ provides a key for the isomer assignments of the various transitions observed in all AnH^+-L_n spectra. The transitions B_i and C_1 are only detected in the 3 → 0 spectrum, whereas the transitions A_i and D_1 are solely observed in the 3 → 1 spectrum. Consequently, both types of transitions, B_i/C_1 and A_i/D_1, can

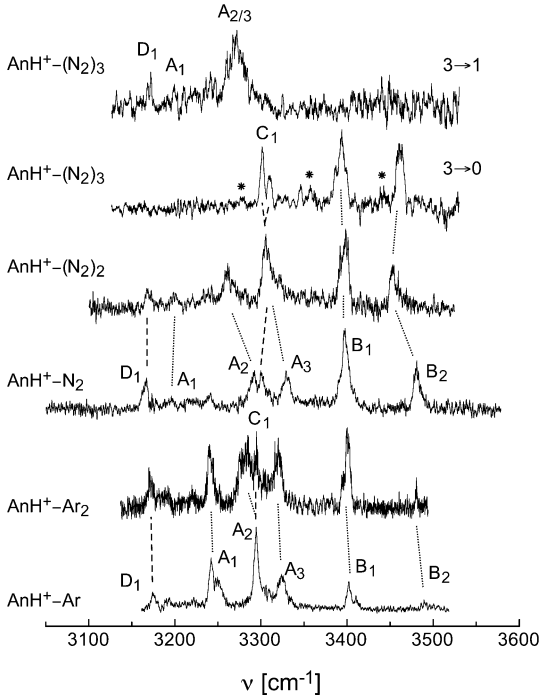

Figure 7. IRPD spectra of AnH^+-L_n for L = Ar ($n = 1, 2$) and L = N_2 ($n = 1-3$) recorded in the range of the N−H stretch fundamentals. The spectra of AnH^+-L_n with $n \leq 2$ are monitored in the AnH^+ channel, whereas $AnH^+-(N_2)_3$ spectra are recorded in both the AnH^+ and the AnH^+-N_2 channels (indicated as 3 → 0 and 3 → 1). The positions and suggested vibrational and isomer assignments of the transitions observed (A_i-D_i) are listed in Table 2. Transitions marked by asterisks arise from $An^+-(N_2)_n$ clusters, which are not fully discriminated by the quadrupole mass spectrometers.

be attributed to (at least) two distinguishable $AnH^+-(N_2)_3$ isomers with different types of AnH^+ ion cores. The AnH^+ isomers involved feature rather different interaction energies with the surrounding N_2 ligands, leading to a different number of ligands evaporated upon single IR photon absorption in the N−H stretch range (3100−3500 cm^{-1}). Indeed, the calculations demonstrate that the ammonium ion **5** features much more acidic N−H bonds than all carbenium ions, leading to lower ν_{NH} frequencies and stronger H bonds to neutral ligands. Consequently, the transitions A_i/D_1 in the 3 → 1 spectrum are assigned to **5**$-(N_2)_3$, whereas the bands B_i/C_1 are attributed to **1/3**$-(N_2)_3$. Similarly, the corresponding transitions observed in the other AnH^+-L_n spectra are assigned to **5**$-L_n$ and **1/3**$-L_n$. The contribution of complexes with the AnH^+ core ions **2** and **4** can be excluded because of their relatively low stability (Figure 2) and their different ν_{NH} frequencies (Figure 5).

On the basis of these arguments, the bands B_1 and B_2 can safely be attributed to the symmetric and antisymmetric N−H stretch modes of **1/3**$-L_n$, ν_{NH}(s) and ν_{NH}(as), respectively. According to the calculations, the properties of the N−H bonds are rather similar for **1**$-L_n$ and **3**$-L_n$. As a consequence, their ν_{NH} frequencies are rather similar as well, which prevents an unambiguous spectroscopic distinction between both cluster isomers in this spectral range. The apparent broadening and the partly resolved splittings in some of the B_1/B_2 bands may be attributed to overlapping transitions of both isomers. Figure 8a compares the experimental ν_{NH}(s,a) frequencies of **1/3**$-L_n$ ($n = 1-3$) with those calculated for **1**$-L_n$ ($n = 0-2$) at the B3LYP/6-31G* level. The latter values are scaled by a factor of 0.9604 obtained by optimizing the agreement between experimental and theoretical values in a least-squares fit. Similar scaling factors have recently been applied to account for the anharmonic effects of N−H stretch frequencies derived at the B3LYP/6-31G* level (0.95663 for An^+, 0.9589 for indole$^+$).[42,43,73] In general, the calculations reproduce qualitatively the complexation-induced frequency shifts. A more quantitative agreement requires calculations at a higher theoretical level to better describe the effects of complexation on both the N−H bond strengths and the coupling between the two N−H stretch oscillators. The derived scaling factor can be employed to estimate the unknown experimental ν_{NH} frequencies of isolated **1/3** as $\nu_{NH}(s) = 3412$ cm^{-1} and $\nu_{NH}(as) = 3518$ cm^{-1} (indicated by filled squares in Figure 8a), respectively. The significant effects of the first two ligands on both N−H stretch frequencies indicate that H bonding to the two available acidic NH_2 protons is indeed the preferred ion−ligand binding motif in **1/3**$-L_n$ clusters with $n \leq 2$. Intermolecular π bonding to the aromatic ring is apparently much less stable. The sequential formation of the H bonds of the first two ligands to the two available acidic NH_2 protons reduces the frequencies of both ν_{NH}(s) and ν_{NH}(as) in each solvation step due to the relatively strong coupling between both N−H stretch local modes. Interestingly, the splitting between ν_{NH}(s) and ν_{NH}(as) increases upon attachment of the third N_2 ligand in **1/3**$-(N_2)_3$ from 56 ($n = 2$) to 68 ($n = 3$) cm^{-1}, indicating that intermolecular π bonding significantly increases the coupling between both N−H stretch modes in **1/3**$-(N_2)_n$ with $n \geq 3$. In general, the trends in the cluster-size-dependent ν_{NH} band shifts of **1/3**$-L_n$ are quite

TABLE 2: Band Maxima and Assignments of Vibrational Transitions Observed in the IRPD Spectra of AnH^+-L_n (Figure 7)

L	*n*	band	position (cm^{-1})	mode	isomer
Ar	1	B_2	3491	ν_{NH}(as)	**1/3**−Ar
		B_1	3402	ν_{NH}(s)	**1/3**−Ar
		A_3	3324	ν_{NH}(3)	**5**−Ar
		A_2	3294	ν_{NH}(2)	**5**−Ar
		C_1	3294	$2\nu_b$	**1/3**−Ar
		A_1	3242	ν_{NH}(1)	**5**−Ar
		D_1	3175	$2\nu_b$	**5**−Ar
	2	B_2	3480	ν_{NH}(as)	**1/3**$-Ar_2$
		B_1	3401	ν_{NH}(s)	**1/3**$-Ar_2$
		A_3	3321	ν_{NH}(3)	**5**$-Ar_2$
		C_1	3294	$2\nu_b$	**1/3**$-Ar_2$
		A_2	3283	ν_{NH}(2)	**5**$-Ar_2$
		A_1	3240	ν_{NH}(1)	**5**$-Ar_2$
		D_1	3172	$2\nu_b$	**5**$-Ar_2$
N_2	1	B_2	3480	ν_{NH}(as)	**1/3**$-N_2$
		B_1	3398	ν_{NH}(s)	**1/3**$-N_2$
		A_3	3329	ν_{NH}(3)	**5**$-N_2$
		C_1	3301	$2\nu_b$	**1/3**$-N_2$
		A_2	3291	ν_{NH}(2)	**5**$-N_2$
		A_1	3195	ν_{NH}(1)	**5**$-N_2$
		D_1	3165	$2\nu_b$	**5**$-N_2$
	2	B_2	3453	ν_{NH}(as)	**1/3**$-(N_2)_2$
		B_1	3397	ν_{NH}(s)	**1/3**$-(N_2)_2$
		C_1	3305	$2\nu_b$	**1/3**$-(N_2)_2$
		A_3	3305	ν_{NH}(3)	**5**$-(N_2)_2$
		A_2	3261	ν_{NH}(2)	**5**$-(N_2)_2$
		A_1	3200	ν_{NH}(1)	**5**$-(N_2)_2$
		D_1	3168	$2\nu_b$	**5**$-(N_2)_2$
	3 (→0)	B_2	3462	ν_{NH}(as)	**1/3**$-(N_2)_3$
		*	3440	ν_{NH}(as)	$An^+-(N_2)_3$
		B_1	3394	ν_{NH}(s)	**1/3**$-(N_2)_3$
		*	3359	ν_{NH}(s)	$An^+-(N_2)_3$
		C_1	3310/3302	$2\nu_b$	**1/3**$-(N_2)_3$
		*	3282	$2\nu_b$	$An^+-(N_2)_3$
	3 (→1)	A_3	3271	ν_{NH}(3)	**5**$-(N_2)_3$
		A_2	3271	ν_{NH}(2)	**5**$-(N_2)_3$
		A_1	3200	ν_{NH}(1)	**5**$-(N_2)_3$
		D_1	3170	$2\nu_b$	**5**$-(N_2)_3$

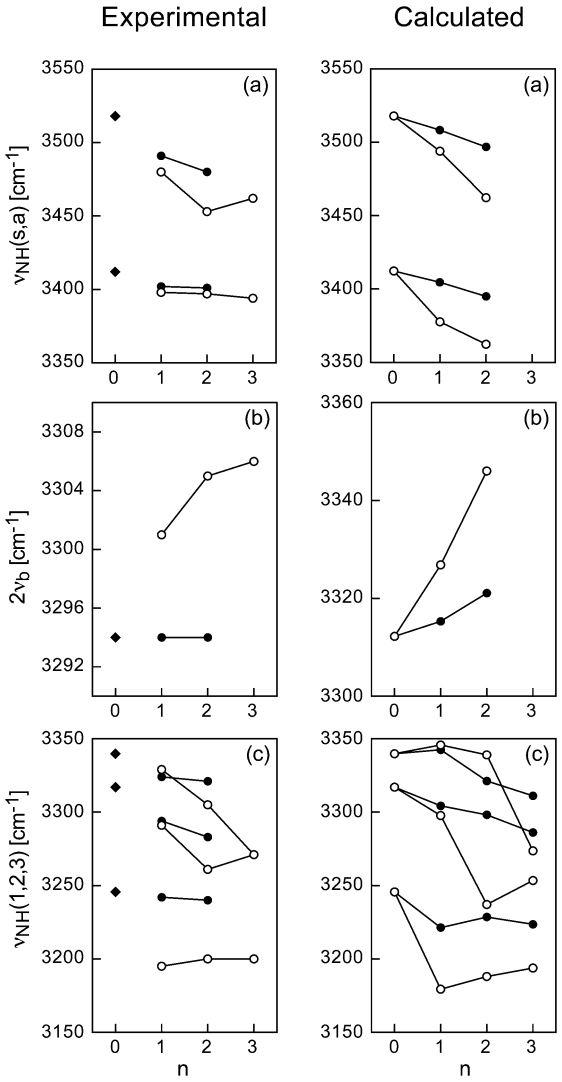

Figure 8. Experimental and calculated vibrational frequencies (B3LYP/6-31G*) of AnH^+-L_n clusters with L = Ar (filled circles) and L = N_2 (open circles) as a function of the cluster size (n): (a) experimental ν_{NH}(s) and ν_{NH}(a) frequencies of **1**/**3**$-L_n$ are compared to calculated values of **1**$-L_n$ (scaling factor of 0.9604); (b) experimental $2\nu_b$ frequencies of **1**/**3**$-L_n$ are compared to calculated values of **1**$-L_n$ (scaling factor of 0.9604); (c) experimental $\nu_{NH}(1-3)$ frequencies of **5**$-L_n$ are compared to calculated values of **5b**$-L_n$ (scaling factor of 0.9620). The scaled theoretical values for $n = 0$ are included in the plots of the experimental data (as filled squares).

similar to those observed previously for the related An^+-L_n radical cation clusters.[42,43]

In addition to the bands B_1 and B_2 assigned to ν_{NH}(s) and ν_{NH}(as) of **1**/**3**$-(N_2)_3$, the 3 → 0 spectrum of $AnH^+-(N_2)_3$ displays a third transition, C_1, which occurs as a doublet at 3302 and 3310 cm^{-1}. This band is assigned to the first overtone of the symmetric in-plane bend vibration of the NH_2 group (scissoring), $2\nu_b$, of **1**/**3**$-(N_2)_3$. The same overtone transition has been detected with high intensity in the IRPD spectra of the related An^+-L_n clusters at $2\nu_b \approx 3270$ cm^{-1}.[42,43] The B3LYP calculations predict harmonic frequencies of $\omega_b = 1676$, 1702, and 1700 cm^{-1} for An^+,[43] **1**, and **3**, respectively. Hence, $2\nu_b$ of **1**/**3** is expected to occur roughly 40−50 cm^{-1} higher in frequency than $2\nu_b$ of An^+, i.e., close to 3310−3320 cm^{-1}, which is in reasonable agreement with the position of band C_1. The small splitting of this transition may again be attributed to $2\nu_b$ of **1**$-(N_2)_3$ and **3**$-(N_2)_3$. It is difficult to unambiguously identify this transition in the spectra of AnH^+-L_n with $n \leq 2$ (see dashed lines in Figure 7), because of spectral overlap of $2\nu_b$ of **1**/**3**$-L_n$ with the N−H stretch fundamentals of **5**$-L_n$ (denoted A_i). As expected, the ν_b frequency is little affected upon π bonding. In general, ν_b increases slightly upon H bonding of ligands to the NH_2 group, because such intermolecular bonds generate additional retarding forces for the NH_2 scissoring motion.[43] Hence, as predicted by the calculations, the frequency of $2\nu_b$ of **1**/**3**$-L_n$ is expected to slightly increase in the order $n = 0 < 1 < 2$ and in the order Ar < N_2. Figure 8b compares the experimental $2\nu_b$ frequencies of **1**/**3**$-L_n$ (n = 1−3) with those calculated for **1**$-L_n$ (n = 0−2) at the B3LYP/6-31G* level ($2\omega_b$ scaled by 0.9604). Again, the calculations reproduce qualitatively the complexation-induced frequency shifts observed experimentally. The best experimental estimate for the frequency for $2\nu_b$ of isolated **1**/**3** is 3294 cm^{-1} (filled square in Figure 8b).

Comparison between the spectra calculated for the AnH^+-Ar isomers involving various AnH^+ ion cores (Figure 6) and the IRPD spectrum of AnH^+-Ar (Figure 7) strongly suggests that the three bands denoted A_i (i = 1−3) in the experimental spectrum arise from the three N−H stretch fundamentals of **5**−Ar, denoted $\nu_{NH}(i)$ with i = 1−3. From the relatively straightforward assignments of $\nu_{NH}(i)$ of **5**−Ar, the corresponding transitions of **5**$-L_n$ can be assigned by comparing the predicted and observed changes in the N−H stretch fundamentals of **5** upon sequential solvation with both Ar and N_2. Figure 8c compares the experimental $\nu_{NH}(1-3)$ frequencies of **5**$-L_n$ (n = 1−3) with the values calculated at the B3LYP/6-31G* level (n = 0−3). The latter ones are scaled by a factor of 0.9620 obtained by optimizing the agreement between experimental and theoretical values in a least-squares fit. This scaling factor can be employed to estimate the unknown experimental $\nu_{NH}(1-3)$ frequencies of bare **5** as 3246, 3317, and 3340 cm^{-1} (indicated by filled squares in Figure 8c), respectively. Again, the calculations reproduce qualitatively the observed complexation-induced frequency shifts, and this agreement supports the conclusion that H bonding to the three available acidic NH_3 protons of **5** is the preferred ion−ligand binding motif in **5**$-L_n$ clusters with $n \leq 3$. Similar to that of **1**/**3**$-L_n$, intermolecular π bonding to the aromatic ring is apparently much less stable than the formation of H bonds. In general, the trends in the cluster-size-dependent ν_{NH} band shifts of **5**$-L_n$ are quite similar to those observed previously for the related $NH_3^+-Ar_n$,[94,95] $NH_4^+-Ar_n$,[87,89−91] and $C_3H_3^+-(N_2)_n$ clusters.[76,98,102]

In addition to the A_i bands (i = 1−3) assigned to the three N−H stretch modes of the ammonium ion in **5**$-(N_2)_3$, the 3 → 1 spectrum of $AnH^+-(N_2)_3$ displays a fourth transition, D_1, at 3170 cm^{-1}. Similar to the A_i bands, D_1 is only seen in the 3 → 1 spectrum and not in the 3 → 0 spectrum. Consequently, band D_1 is also attributed to the **5**$-(N_2)_3$ isomer of $AnH^+-(N_2)_3$, and comparison with the B3LYP calculations strongly suggests an assignment to the first overtone of a scissoring-type N−H bend motion of the NH_3 group, $2\nu_b$. The calculations predict the harmonic frequency of this N−H bend mode of **5** (ω_b) to be ∼1650 cm^{-1}, i.e., around 50 cm^{-1} below that of the corresponding scissoring mode of **1**/**3** (Table 1). Hence, $2\nu_b$ of **5** is expected to occur roughly 100 cm^{-1} lower in frequency than $2\nu_b$ of **1**/**3**. The latter transition corresponds to band C_1 of **1**/**3**, which is observed around 3300 cm^{-1} in the IRPD spectra of **1**/**3**$-L_n$. Hence, $2\nu_b$ of **5**$-L_n$ is predicted to be around 3200 cm^{-1}, in reasonable agreement with band D_1 observed in the spectra of AnH^+-L_n (Figure 7, Table 2). Similar to that of $2\nu_b$

TABLE 3: Comparison between Experimental and Calculated Dissociation Energies of AnH^+-N_2 Isomers

isomer	D_0 (cm^{-1})	D_e[a] (cm^{-1})
1/**3**$-N_2(\pi)$	800 ± 300	
1/**3**$-N_2$(H)	950 ± 450	895/907
5$-N_2$(H)	1400 ± 300	1370

[a] Evaluated at the B3LYP/6-31G* level.

of **1**/**3**$-L_n$, the frequency of $2\nu_b$ of **5**$-L_n$ is very little affected by complexation.

Photofragmentation Channels and Binding Energies. After assignment of the vibrational transitions of the various AnH^+-L_n isomers, the photofragmentation branching ratios are evaluated. According to eq 3, several AnH^+-L_m fragment channels may be observed for a given AnH^+-L_n parent complex with $n > 1$. The number of ligands evaporated upon single-photon absorption depends sensitively on the ligand type (Ar, N_2), the size of the complex (n), and the AnH^+ isomer acting as the cation core in AnH^+-L_n. Previous studies on related cluster systems using the same experimental setup have demonstrated that the range of observed fragment channels (m) is rather narrow. This information has been employed to roughly estimate ion−ligand binding energies using a simple model described in detail elsewhere.[44,70,72,103] The basic assumption of this model is that the total energy of the absorbed IR photon can be used to sequentially evaporate the most weakly bound ligands in the complex. Furthermore, the ligands are classified into H-bound and π-bound ones, with dissociation energies of $D_0(H) > D_0(\pi)$, respectively. The observation that a photon energy of 3300 cm^{-1} is sufficient to evaporate two but not three H-bound N_2 ligands of **5**$-(N_2)_3$ implies $D_0(H) \approx 1400 \pm 300$ cm^{-1}, in good agreement with $D_e(H) = 1370$ cm^{-1} calculated for H-bound **5**$-N_2$. The photon energy of 3300 cm^{-1} is sufficient to evaporate all three ligands of **1**/**3**$-(N_2)_3$, giving rise to the relation $2D_0(H) + D_0(\pi) < 3300$ cm^{-1}. Together with the condition $D_0(H) > D_0(\pi)$, this relation results in $D_0(\pi) < 1100$ cm^{-1}. Previous experimental data showed that $D_0(\pi)$ of N_2 complexed to an aromatic cation is relatively insensitive to the type of aromatic ion and on the order of 500−1100 cm^{-1}.[16,44] For example, $D_0(\pi) = 700 \pm 200$ cm^{-1} for An^+-N_2.[43] Under the realistic assumption that $D_0(\pi) > 500$ cm^{-1} also for **1**/**3**$-N_2$, $D_0(\pi)$ can be bracketed as 800 ± 300 cm^{-1}. This estimate enables $D_0(H)$ of **1**/**3**$-(N_2)_3$ to be determined as 950 ± 450 cm^{-1}, again consistent with $D_e(H) = 895$ and 907 cm^{-1} calculated for H-bound **1**$-N_2$ and **3**$-N_2$, respectively. The available experimental and calculated dissociation energies of isomeric AnH^+-N_2 dimers are summarized in Table 3. The corresponding binding energy data for **1**/**3**−Ar and **5**−Ar derived from the IRPD spectra of AnH^+-Ar_n ($n \leq 2$) are much less informative. Essentially, the spectra provide only upper limits for $D_0(H)$ of **1**/**3**−Ar and **5**−Ar as 1600 and 1700 cm^{-1}, respectively.

Further Discussion

The IRPD spectra of AnH^+-L_n reveal the unambiguous spectroscopic fingerprints of (at least) two different AnH^+ isomers in the supersonic plasma expansion: the ammonium isomer (**5**) and the para- and/or ortho-protonated carbenium isomers (**1**/**3**). Complexes of meta-protonated (**2**) and ipso-protonated (**4**) aniline are not observed. Thus, in line with the theoretical predictions, the IR spectra demonstrate that **2** and **4** are substantially less stable than **1**/**3** and **5**. It is difficult to infer from the IRPD spectra further quantitative conclusions about the relative stabilities of the observed AnH^+ isomers, because several factors affect the relative intensities of the observed vibrational transitions,[13,18] including (i) the production ratio for the bare AnH^+ isomers, (ii) their efficiency to form AnH^+-L_n clusters, and (iii) the IR oscillator strengths. Previous experiments on protonated phenol showed that the production ratio for the bare protonated phenol isomers can strongly depend on the experimental conditions, such as the composition or pressure of the expansion gas.[18] Thus, the AnH^+ isomer ratio is not only controlled by energetic but also by kinetic factors. As **1**, **3**, and **5** are separated from each other by large isomerization barriers, they can be collisionally stabilized in a wide range of abundance ratios, which sensitively depend on the expansion conditions. Similarly, even for a given AnH^+ isomer ratio, the resulting AnH^+-L_n cluster ratio will depend on the relative efficiency for cluster formation, which again is controlled by both thermodynamic and entropic factors. For example, the stronger intermolecular H bonds in **5**$-L_n$ compared to those in **1**/**3**$-L_n$ will favor the detection of the former over the latter complexes.

TABLE 4: Estimated Experimental Vibrational Frequencies of Selected AnH^+ Isomers (cm^{-1})[a]

isomer	vibration	frequency	isomer	vibration	frequency
1/**3**	ν_{NH}(s)	3412	**5**	$\nu_{NH}(1)$	3246
	ν_{NH}(a)	3518		$\nu_{NH}(2)$	3317
	$2\nu_b$	3294		$\nu_{NH}(3)$	3340
				$2\nu_b$	3170

[a] Extrapolated from IRPD spectra of AnH^+-L_n to zero solvation conditions ($n = 0$, Figure 8).

The IR spectra of AnH^+-L_n allow for an accurate extrapolation of the N−H stretch and bend frequencies of the isolated AnH^+ isomers **1**/**3** and **5** by comparison to theoretical calculations and extrapolation to zero solvation ($n = 0$, Figure 8). The results obtained are compared in Table 4. The center frequencies ($\nu_{NH,av}$) of ν_{NH}(s) and ν_{NH}(as) of **1**/**3** and $\nu_{NH}(1)$, $\nu_{NH}(2)$, and $\nu_{NH}(3)$ of **5** provide a measure for the N−H bond strength in both types of AnH^+ isomers. The experimental estimates of $\nu_{NH,av} = 3465$ and 3301 cm^{-1} for **1**/**3** and **5** are in accord with the corresponding theoretical values of $\omega_{NH,av} = 3607$ and 3436 cm^{-1} (Table 1), respectively. The difference of around 170 cm^{-1} in $\nu_{NH,av}$ confirms that the N−H bonds in **5** are much weaker and more acidic than those in **1**/**3**. Comparison with the average N−H stretch frequencies of neutral aniline and the aniline radical cation, $\nu_{NH,av} = 3464.5$ and 3439.5 cm^{-1},[40] reveals that the N−H bond strength varies in the order An ≈ **1**/**3** > An^+ > **5**. These observation are in line with the variations in calculated N−H bond lengths, $R_{NH,av}/Å = 1.0073 \approx 1.0093 < 1.0108 < 1.0273$, and harmonic stretch frequencies, $\omega_{NH,av}/cm^{-1} = 3609.5 \approx 3607 > 3591 > 3436$ (Table 1). Apparently, ionization of An slightly weakens the N−H bonds, protonation at the ring in the ortho and para positions has nearly no effect, and protonation at the N atom leads to a large destabilization. Comparison of **5** with NH_4^+ reveals the effects of substitution of a H atom by a phenyl group on the acidity of the ammonium ion. The averaged frequency of the N−H stretch fundamentals of NH_4^+, $\nu_{NH,av} \approx 3318$ cm^{-1},[104,105] is slightly larger than the value for **5**, $\nu_{NH,av} \approx 3301$ cm^{-1}, an indication that H → C_6H_5 substitution has a destabilizing effect on the N−H bonds. This observation is consistent with the calculated values for R_{NH} (1.0240 vs 1.0273 Å) and $\omega_{NH,av}$ (3450 vs 3436 cm^{-1}) for NH_4^+ and **5**, respectively.

The significant cluster-size-dependent frequency shifts of the N−H stretch modes demonstrate that the microsolvation sequence of **1**/**3** and **5** with Ar and N_2 ligands begins with the solvation of all available NH protons and proceeds by the

formation of intermolecular π bonds. Related complexes of substituted $A(H)^+$ ions featuring an acidic YH_k group, such as A = phenol and naphthol (YH_k = OH),[72,74] aniline (YH_k = NH_2),[42,43] and imidazole[36] and indole[73] (YH_k = NH), show a very similar cluster growth. The available *k* acidic proton(s) of the YH_k group are solvated first, and π bonds are formed subsequently. In contrast to these substituted $A(H)^+$ ions, small cluster ions of A = benzene with nonpolar ligands show exclusively intermolecular π bonding.[15,16,106] Hence, H bonds of nonpolar ligands to CH_2 and CH groups of $A(H)^+$ ions are generally less stable than H bonds to acidic YH_k groups and π bonds to the aromatic rings. Previous IRPD experiments on small, nonaromatic cluster ions of the type $XH_k^+-L_n$ with nonpolar ligands (L = Rg, N_2, H_2), such as XH_k^+ = OH^+,[107] OCH^+,[99,103,108] N_2H^+,[109−112] O_2H^+,[113] $SiOH^+$,[100,114] $OCOH^+$,[115] NH_2^+,[116−118] NH_3^+,[94,95] NH_4^+,[87] and H_2O^+,[96,119−121] revealed that the first *k* ligands in $XH_k^+-L_n$ form strong intermolecular XH^+-L proton bonds before other and less stable binding sites are occupied. These systematic studies also showed that the strengths of the intermolecular XH^+-L proton bonds are correlated with the proton affinities of both bases X and L.[97,100,108] As the proton affinity of Ar is lower than that of N_2 (369 < 494 kJ/mol),[84] the intermolecular H bonds in AnH^+-Ar_n are weaker than those in $AnH^+-(N_2)_n$.

Comparison of $An-L_n$, An^+-L_n, and AnH^+-L_n clusters with L = Ar and N_2 reveals the drastic effect of both ionization and protonation on the preferred recognition motif between these prototypical arylamines and nonpolar solvent molecules. Neutral An−Ar and An−N_2 dimers prefer intermolecular π bonding in the ground electronic state,[38−41] because dispersion interactions between An and L provide the dominant contribution to the attractive part of the intermolecular potential. H-bound An−Ar and An−N_2 isomers have not been detected so far. The topology of the interaction potentials of An^+-L and AnH^+-L differs qualitatively from that of neutral An−L, because of the significant additional electrostatic and inductive attraction arising from the excess positive charge. As a consequence, the An^+-L and AnH^+-L complexes with Ar and N_2 prefer H bonding over π bonding, demonstrating the large impact of protonation and ionization on the most stable binding motif. A similar $\pi \rightarrow$ H switch in the aromatic molecule−solvent recognition induced by ionization or protonation has recently been observed for a variety of acidic aromatic molecules (phenol, indole, imidazole, naphthol) interacting with nonpolar ligands (see ref 44 for a detailed review on this topic). Very recently, the dynamics of this charge-induced $\pi \rightarrow$ H switch from hydrophobic to hydrophilic recognition has been probed for the first time in real time by picosecond pump−probe spectroscopy of the prototypical phenol−Ar interaction, yielding a time constant on the order of 5−10 ps for this fundamental intermolecular isomerization process.[122]

Concluding Remarks

IRPD spectra of size-selected AnH^+-L_n complexes (L = Ar, N_2; $n \leq 3$) are analyzed in the N−H stretch range to probe the protonation sites of aniline and the subsequent microsolvation process of AnH^+ in an inert solvent. The spectra obtained correspond to the first spectroscopic data for clusters with protonated aniline as a chromophore. Thus, they provide a first impression of the biophysically relevant potential energy surface of protonated arylamines interacting with neutral molecules. In addition, the spectra present the first spectroscopic attempt to unambiguously determine the protonation sites observed for isolated and microsolvated AnH^+. The analysis of the vibrational frequencies and photofragmentation data of AnH^+-L_n confirms the simultaneous production of two different types of AnH^+ isomers in the employed plasma expansion of An, H_2, and L, namely, the anilinium ion **5** and the carbenium ions **1**/**3**. There is no evidence for the generation of the other carbenium isomers **2** and **4**, which are predicted to be significantly less stable species on the AnH^+ potential energy surface than **1**/**3** and **5**. The different AnH^+ isomeric core ions in the AnH^+-L_n clusters are identified not only by their different vibrational frequencies but also by their different photofragmentation behaviors. The vibrational spectra demonstrate that the preferred microsolvation sequence of both **1**/**3** and **5** in both Ar and N_2 is characterized by first forming intermolecular H bonds of L to all available acidic N−H protons and then forming π bonds to the six-membered rings. Both the photofragmentation ratios and the N−H stretch frequencies demonstrate that the N−H bonds in **5** are significantly weaker than in **1**/**3**, resulting in stronger H bonds to the neutral solvent molecules. This observation corresponds to the first spectroscopic probe of the acidity of the NH protons of the various AnH^+ isomers under isolated and microsolvation conditions. In general, protonation of aniline induces chemically significant changes of the properties of its N−H bonds, and the magnitude of the effects strongly depend on the protonation site. While protonation in the ortho and para positions has nearly no impact on the N−H bonds, they become much longer, weaker, and more acidic for protonation at the N atom. Thus, the present data on weak stepwise solvation provide a quantitative molecular level explanation for the known observation that aniline prefers protonation at the N atom in the condensed phase. Comparison with clusters of neutral An and the An^+ radical cation demonstrates the drastic effect of protonation and ionization on the acidity of the N−H groups and the topology of the intermolecular potential, in particular on the preferred aromatic substrate−nonpolar ligand recognition motif. Whereas neutral An−L dimers with L = Ar and N_2 prefer π bonding of L to the aromatic ring, H bonding to the acidic NH protons is the most stable binding site in AnH^+-L and An^+-L. In many aspects, the protonation and subsequent microsolvation processes of aniline are similar to those of isoelectronic phenol. Moreover, the AnH^+-L_n spectra demonstrate that the IRPD process can be employed in an elegant way to prepare a spectroscopically clean ion beam of selected AnH^+ isomers (for example, either **5** or **1**/**3**) because of their different photofragmentation behaviors. Such an isomer-clean ion beam may subsequently be assayed by the large body of mass spectrometric techniques available to probe the different reactivities of isomer-selected **5** or **1**/**3** toward a variety of neutral molecular reactants. Future studies aim at the characterization of the protonation process of aniline as a function of the degree of microhydration to characterize the interaction of protonated arylamines with a controlled number of water ligands. Such interactions may be relevant for biophysical processes where protonated biomolecular building blocks containing aromatic rings and amino groups interact with a limited number of water molecules. Other future directions include the measurement of IRMPD spectra of AnH^+ in the fingerprint range using a free electron laser (500−2000 cm^{-1}) as well as IR(M)PD spectra of AnH^+ (clusters) generated by different techniques to prepare selectively a single AnH^+ isomer.[56]

Acknowledgment. This study was supported by the Deutsche Forschungsgemeinschaft (Grant DO 729/2) and the Fonds der Chemischen Industrie. Part of this work is taken from a project thesis of F.M.P. (University of Würzburg, 2004).

References and Notes

(1) Carey, F. A.; Sundberg, R. J. *Advanced Organic Chemistry*; Plenum Press: New York, 1995.

(2) Smith, M. B.; March, J. *Advanced Organic Chemistry: Reactions, Mechanisms, and Structure*, 5th ed.; Wiley: New York, 2001.

(3) Stewart, R. *The Proton: Applications to Organic Chemistry*; Academic Press: New York, 1985.

(4) Olah, G. A. *Acc. Chem. Res.* **1971**, *4*, 240.

(5) Olah, G. A.; White, A. M.; O'Brien, D. H. *Chem. Rev.* **1970**, *70*, 561.

(6) Koptyug, V. A. *Top. Curr. Chem.* **1984**, *122*, 1.

(7) Lenoir, D. *Angew. Chem., Int. Ed.* **2003**, *42*, 854.

(8) Fornarini, S. *Mass Spectrom. Rev.* **1996**, *15*, 365.

(9) Fornarini, S.; Crestoni, M. E. *Acc. Chem. Res.* **1998**, *31*, 827.

(10) Kuck, D. *Mass Spectrom. Rev.* **1990**, *9*, 583.

(11) Chiavarino, B.; Crestoni, M. E.; Fornarini, S. *J. Phys. Org. Chem.* **2004**, *17*, 957.

(12) Solcà, N.; Dopfer, O. *J. Am. Chem. Soc.* **2003**, *125*, 1421.

(13) Solcà, N.; Dopfer, O. *Chem. Phys. Lett.* **2001**, *342*, 191.

(14) Dopfer, O. *J. Phys. Org. Chem.* DOI: 10.1002/poc.1053.

(15) Solcà, N.; Dopfer, O. *Angew. Chem., Int. Ed.* **2002**, *41*, 3628.

(16) Solcà, N.; Dopfer, O. *Chem.—Eur. J.* **2003**, *9*, 3154.

(17) Chaudhuri, C.; Wu, C.-C.; Jiang, J.-C.; Chang, H.-C. *Aust. J. Chem.* **2004**, *57*, 1153.

(18) Solcà, N.; Dopfer, O. *J. Am. Chem. Soc.* **2004**, *126*, 1716.

(19) Solcà, N.; Dopfer, O. *J. Chem. Phys.* **2004**, *120*, 10470.

(20) Solcà, N.; Dopfer, O. *J. Chem. Phys.* **2004**, *121*, 769.

(21) Solcà, N.; Dopfer, O. *Angew. Chem., Int. Ed.* **2003**, *42*, 1537.

(22) Solcà, N.; Dopfer, O. *ChemPhysChem* **2005**, *6*, 434.

(23) Andrei, H. S.; Solcà, N.; Dopfer, O. *ChemPhysChem* **2006**, *7*, 107.

(24) Kamariotis, A.; Boyarkin, O. V.; Mercier, S.; Bush, M. F.; Williams, E. R.; Beck, R. D.; Rizzo, T. R. *J. Am. Chem. Soc.* **2006**, *128*, 905.

(25) Jones, W.; Boissel, P.; Chiavarino, B.; Crestoni, M. E.; Fornarini, S.; Lemaire, J.; Maitre, P. *Angew. Chem., Int. Ed.* **2003**, *42*, 2057.

(26) Chiavarino, B.; Crestoni, M. E.; Fornarini, S.; Lemaire, J.; MacAleese, L.; Maitre, P. *ChemPhysChem* **2005**, *6*, 437.

(27) Oomens, J.; von Helden, G.; Meijer, G. *J. Phys. Chem. A* **2004**, *108*, 8273.

(28) Oomens, J.; von Helden, G.; Meijer, G. *Int. J. Mass Spectrom.* **2006**, *249*−*250*, 199.

(29) Dopfer, O.; Solcà, N.; Lemaire, J.; Maitre, P.; Crestoni, M. E.; Fornarini, S. *J. Phys. Chem. A* **2005**, *109*, 7881.

(30) Dopfer, O.; Lemaire, J.; Maitre, P.; Crestoni, M. E.; Fornarini, S. *Int. J. Mass Spectrom.* **2006**, *249*−*250*, 149.

(31) Chiavarino, B.; Crestoni, M. E.; Fornarini, S.; Dopfer, O.; Lemaire, J.; Maitre, P. *J. Phys. Chem. A* **2006**, *110*, 9352.

(32) Oomens, J.; Sartakov, B. G.; Meijer, G.; von Helden, G. *Int. J. Mass Spectrom.* **2006**, *252*, 1.

(33) Olah, G. A.; Kelly, D. P.; Dunne, K.; Mo, Y. K. *J. Am. Chem. Soc.* **1972**, *94*, 7438.

(34) Bagno, A.; Terrier, F. *J. Phys. Chem. A* **2001**, *105*, 6537.

(35) Tajima, S.; Shiobara, S.; Shizuka, H.; Tobita, S. *Phys. Chem. Chem. Phys.* **2002**, *4*, 3376.

(36) Andrei, H. S.; Solcà, N.; Dopfer, O. *J. Phys. Chem. A* **2005**, *109*, 3598.

(37) Solcà, N.; Dopfer, O. *J. Mol. Struct.* **2001**, *563/564*, 241.

(38) Sinclair, W. E.; Pratt, D. W. *J. Chem. Phys.* **1996**, *105*, 7942.

(39) Schäfer, M.; Pratt, D. W. *J. Chem. Phys.* **2001**, *115*, 11147.

(40) Honda, M.; Fujii, A.; Fujimaki, E.; Ebata, T.; Mikami, N. *J. Phys. Chem. A* **2003**, *107*, 3678.

(41) Piest, H.; von Helden, G.; Meijer, G. *J. Chem. Phys.* **1999**, *110*, 2010.

(42) Solcà, N.; Dopfer, O. *Eur. Phys. J. D* **2002**, *20*, 469.

(43) Solcà, N.; Dopfer, O. *J. Phys. Chem. A* **2002**, *106*, 7261.

(44) Dopfer, O. *Z. Phys. Chem.* **2005**, *219*, 125.

(45) Heidrich, D. *Angew. Chem., Int. Ed.* **2002**, *41*, 3208.

(46) Amunugama, R.; Rodgers, M. T. *Int. J. Mass Spectrom.* **2003**, *227*, 339.

(47) Moore, D. T.; Oomens, J.; Eyler, J. R.; von Helden, G.; Meijer, G.; Dunbar, R. C. *J. Am. Chem. Soc.* **2005**, *127*, 7243.

(48) Oomens, J.; Moore, D. T.; von Helden, G.; Meijer, G.; Dunbar, R. C. *J. Am. Chem. Soc.* **2004**, *126*, 724.

(49) Ma, J. C.; Dougherty, D. A. *Chem. Rev.* **1997**, *97*, 1303.

(50) Ranasinghe, Y. A.; Glish, G. L. *J. Am. Soc. Mass Spectrom.* **1996**, *7*, 473.

(51) Hillebrand, C.; Klessinger, M.; EckertMaksic, M.; Maksic, Z. B. *J. Phys. Chem.* **1996**, *100*, 9698.

(52) Roy, R. K.; de Proft, F.; Geerlings, P. *J. Phys. Chem. A* **1998**, *102*, 7035.

(53) Russo, N.; Toscano, M.; Grand, A.; Mineva, T. *J. Phys. Chem. A* **2000**, *104*, 4017.

(54) Lee, S.-W. C., H.; Goddard, W. A., III; Beauchamp, J. L. *J. Am. Chem. Soc.* **2000**, *122*, 9201.

(55) Le, H. T.; Flammang, R.; Barbieux-Flammang, M.; Gerbaux, P.; Nguyen, M. T. *Int. J. Mass Spectrom.* **2002**, *217*, 45.

(56) Flammang, R.; Dechamps, N.; Pascal, L.; Van Haverbeke, Y.; Gerbaux, P.; Nam, P. C.; Nguyen, M. T. *Lett. Org. Chem.* **2004**, *1*, 23.

(57) Wiberg, K. B. *Collect. Czech. Chem. Commun.* **2004**, *69*, 2183.

(58) Lau, Y. K.; Nishizawa, K.; Tse, A.; Brown, R. S.; Kebarle, P. *J. Am. Chem. Soc.* **1981**, *103*, 6291.

(59) Bagno, A. B., B.; Bertrand, S.; Comuzzi, C.; Dorigo, F.; Janvier, P.; Scorrano, G. *Chem.—Eur. J.* **1999**, *5*, 523.

(60) Summerhays, K. D.; Pollack, S. K.; Taft, R. W.; Hehre, W. J. *J. Am. Chem. Soc.* **1977**, *99*, 4585.

(61) Pollack, S. K.; Devlin, J. L.; Summerhays, K. D.; Taft, R. W.; Hehre, W. J. *J. Am. Chem. Soc.* **1977**, *99*, 4583.

(62) Lau, Y. K.; Saluja, P. P. S.; Kebarle, P.; Alder, R. W. *J. Am. Chem. Soc.* **1978**, *100*, 7328.

(63) Lau, Y. K.; Kebarle, P. *J. Am. Chem. Soc.* **1976**, *98*, 7452.

(64) Wood, K. V.; Burinsky, D. J.; Cameron, D.; Cooks, R. G. *J. Org. Chem.* **1983**, *48*, 5236.

(65) Pachuta, S. J.; Isernflecha, I.; Cooks, R. G. *Org. Mass Spectrom.* **1986**, *21*, 1.

(66) Smith, R. L.; Chyall, L. J.; Beasley, B. J.; Kenttämaa, H. I. *J. Am. Chem. Soc.* **1995**, *117*, 7971.

(67) Nold, M. J.; Wesdemiotis, C. *J. Mass Spectrom.* **1996**, *31*, 1169.

(68) Ranasinghe, Y. A.; Glish, G. L. *Int. J. Mass Spectrom.* **1999**, *191*, 295.

(69) Harrison, A. G.; Tu, Y. P. *Int. J. Mass Spectrom.* **2000**, *196*, 33.

(70) Dopfer, O. *Int. Rev. Phys. Chem.* **2003**, *22*, 437.

(71) Solcà, N.; Dopfer, O. *J. Phys. Chem. A* **2005**, *109*, 6174.

(72) Solcà, N.; Dopfer, O. *J. Phys. Chem. A* **2001**, *105*, 5637.

(73) Solcà, N.; Dopfer, O. *Phys. Chem. Chem. Phys.* **2004**, *6*, 2732.

(74) Andrei, H. S.; Solcà, N.; Dopfer, O. *Phys. Chem. Chem. Phys.* **2004**, *6*, 3801.

(75) Solcà, N.; Dopfer, O. *Chem. Phys. Lett.* **2001**, *347*, 59.

(76) Dopfer, O.; Roth, D.; Maier, J. P. *Int. J. Mass. Spectrom.* **2002**, *218*, 281.

(77) Guelachvili, G.; Rao, K. N. *Handbook of Infrared Standards*; Academic Press: London, 1993; Vols. 1 and 2.

(78) Frisch, M. J.; Trucks, G. W.; Schlegel, H. B.; Scuseria, G. E.; Robb, M. A.; Cheeseman, J. R.; Montgomery, J. A.; Vreven, T.; Kudin, K. N.; Burant, J. C.; Millam, J. M.; Iyengar, S. S.; Tomasi, J.; Barone, V.; Menucci, B.; Cossi, M.; Scalmani, G.; Rega, N.; Petersson, G. A.; Nakatsuji, H.; Hada, M.; Ehara, M.; Toyota, K.; Fukuda, R.; Hasegawa, J.; Ishida, M.; Nakajima, T.; Honda, Y.; Kitao, O.; Nakai, H.; Klene, M.; Li, X.; Knox, J. E.; Hratchian, H. P.; Cross, J. B.; Adamo, C.; Jaramillo, J.; Gomperts, R.; Stratman, R. E.; Yazyev, P. Y.; Austin, A. J.; Cammi, R.; Pomelli, C.; Ochterski, J.; Ayala, P. Y.; Morokuma, K.; Voth, G. A.; Salvador, P.; Dannenberg, J. J.; Zakrzewski, V. G.; Dapprich, S.; Daniels, A. D.; Strain, M. C.; Farkas, O.; Malick, D. K.; Rabuck, D.; Raghavachari, K.; Foresman, J. B.; Ortiz, J. V.; Cui, Q.; Baboul, A. G.; Clifford, S.; Cioslowski, J.; Stefanov, B. B.; Liu, G.; Liashenko, A.; Piskorz, P.; Komaromi, I.; Martin, R. L.; Fox, D. J.; Keith, T.; Al-Laham, M. A.; Peng, C. Y.; Nanayakkara, A.; Gonzales, C.; Challacombe, M.; Gill, P. M. W.; Johnson, B. G.; Chen, W.; Wong, M. W.; Gonzales, C.; Pople, J. A. *Gaussian 03*, Revision B.01; Gaussian, Inc.: Pittsburgh, PA, 2003.

(79) Solcà, N.; Dopfer, O. *Chem. Phys. Lett.* **2000**, *325*, 354.

(80) Boys, S. F.; Bernardi, F. *Mol. Phys.* **1970**, *19*, 553.

(81) Heidrich, D.; Deininger, D. *Tetrahedron Lett.* **1977**, *18*, 3751.

(82) Rudolph, H. D.; Dreizler, H.; Jaeschke, A.; Wendling, P. *Z. Naturforsch., A: Astrophys., Phys. Phys. Chem.* **1967**, *A22*, 940.

(83) Kreiner, W. A.; Rudolph, H. D.; Tan, B. T. *J. Mol. Spectrosc.* **1973**, *48*, 86.

(84) Hunter, E. P. L.; Lias, S. G. *J. Phys. Chem. Ref. Data* **1998**, *27*, 413.

(85) Solcà, N.; Dopfer, O. *Chem. Phys. Lett.* **2003**, *369*, 68.

(86) Fujii, A.; Miyazaki, M.; Ebata, T.; Mikami, N. *J. Chem. Phys.* **1999**, *110*, 11125.

(87) Dopfer, O.; Nizkorodov, S. A.; Meuwly, M.; Bieske, E. J.; Maier, J. P. *Int. J. Mass Spectrom. Ion Processes* **1997**, *167*−*168*, 637.

(88) Lakin, N. M.; Olkhov, R. V.; Dopfer, O. *Faraday Discuss.* **2001**, *118*, 455.

(89) Lakin, N. M.; Dopfer, O.; Meuwly, M.; Howard, B. J.; Maier, J. P. *Mol. Phys.* **2000**, *98*, 63.

(90) Lakin, N. M.; Dopfer, O.; Howard, B. J.; Maier, J. P. *Mol. Phys.* **2000**, *98*, 81.

(91) Bieske, E. J.; Nizkorodov, S. A.; Dopfer, O.; Maier, J. P.; Stickland, R. J.; Cotterell, B. J.; Howard, B. J. *Chem. Phys. Lett.* **1996**, *250*, 266.

(92) Dopfer, O.; Nizkorodov, S. A.; Meuwly, M.; Bieske, E. J.; Maier, J. P. *Chem. Phys. Lett.* **1996**, *260*, 545.

(93) Meuwly, M.; Nizkorodov, S. A.; Bieske, E. J.; Maier, J. P.; Dopfer, O. *Chem. Phys. Lett.* **1997**, *270*, 252.

(94) Dopfer, O. *Chem. Phys.* **2002**, *283*, 63.

(95) Dopfer, O.; Solcà, N.; Olkhov, R. V.; Maier, J. P. *Chem. Phys.* **2002**, *283*, 85.
(96) Dopfer, O. *J. Phys. Chem. A* **2000**, *104*, 11693.
(97) Bieske, E. J.; Dopfer, O. *Chem. Rev.* **2000**, *100*, 3963.
(98) Roth, D.; Dopfer, O. *Phys. Chem. Chem. Phys.* **2002**, *4*, 4855.
(99) Olkhov, R. V.; Nizkorodov, S. A.; Dopfer, O. *J. Chem. Phys.* **1997**, *107*, 8229.
(100) Olkhov, R. V.; Dopfer, O. *Chem. Phys. Lett.* **1999**, *314*, 215.
(101) Solcà, N.; Dopfer, O. *J. Am. Chem. Soc.* **2004**, *126*, 9520.
(102) Dopfer, O.; Roth, D.; Maier, J. P. *J. Am. Chem. Soc.* **2002**, *124*, 494.
(103) Nizkorodov, S. A.; Dopfer, O.; Ruchti, T.; Meuwly, M.; Maier, J. P.; Bieske, E. J. *J. Phys. Chem.* **1995**, *99*, 17118.
(104) Jacox, M. E.; Thompson, W. E. *Phys. Chem. Chem. Phys.* **2005**, *7*, 768.
(105) Martin, J. M. L.; Lee, T. J. *Chem. Phys. Lett.* **1996**, *258*, 129.
(106) Dopfer, O.; Olkhov, R. V.; Maier, J. P. *J. Chem. Phys.* **1999**, *111*, 10754.
(107) Roth, D.; Nizkorodov, S. A.; Maier, J. P.; Dopfer, O. *J. Chem. Phys.* **1998**, *109*, 3841.
(108) Nizkorodov, S. A.; Dopfer, O.; Meuwly, M.; Maier, J. P.; Bieske, E. J. *J. Chem. Phys.* **1996**, *105*, 1770.
(109) Dopfer, O.; Olkhov, R. V.; Maier, J. P. *J. Phys. Chem. A* **1999**, *103*, 2982.
(110) Nizkorodov, S. A.; Meuwly, M.; Maier, J. P.; Dopfer, O.; Bieske, E. J. *J. Chem. Phys.* **1998**, *108*, 8964.
(111) Meuwly, M.; Nizkorodov, S. A.; Maier, J. P.; Bieske, E. J. *J. Chem. Phys.* **1996**, *104*, 3876.
(112) Nizkorodov, S. A.; Spinelli, Y.; Bieske, E. J.; Maier, J. P.; Dopfer, O. *Chem. Phys. Lett.* **1997**, *265*, 303.
(113) Nizkorodov, S. A.; Roth, D.; Olkhov, R. V.; Maier, J. P.; Dopfer, O. *Chem. Phys. Lett.* **1997**, *278*, 26.
(114) Olkhov, R. V.; Nizkorodov, S. A.; Dopfer, O. *Chem. Phys.* **1998**, *239*, 393.
(115) Dopfer, O.; Olkhov, R. V.; Roth, D.; Maier, J. P. *Chem. Phys. Lett.* **1998**, *296*, 585.
(116) Dopfer, O.; Nizkorodov, S. A.; Olkhov, R. V.; Maier, J. P.; Harada, K. *J. Phys. Chem. A* **1998**, *102*, 10017.
(117) Dopfer, O.; Roth, D.; Maier, J. P. *Chem. Phys. Lett.* **1999**, *310*, 201.
(118) Roth, D.; Dopfer, O.; Maier, J. P. *Phys. Chem. Chem. Phys.* **2000**, *2*, 5013.
(119) Roth, D.; Dopfer, O.; Maier, J. P. *Phys. Chem. Chem. Phys.* **2001**, *3*, 2400.
(120) Dopfer, O.; Roth, D.; Maier, J. P. *J. Chem. Phys.* **2001**, *114*, 7081.
(121) Dopfer, O.; Engel, V. *J. Chem. Phys.* **2004**, *121*, 12345.
(122) Ishiuchi, S.; Sakai, M.; Tsuchida, Y.; Takeda, A.; Kawashima, Y.; Fujii, M.; Dopfer, O.; Müller-Dethlefs, K. *Angew. Chem., Int. Ed.* **2005**, *44*, 6149.
(123) Linstrom, P. J.; Mallard, W. G. *NIST Chemistry WebBook*; NIST Standards and Technology: Gaithersburg, MD, 2001; http://webbook.nist.gov.